

General and Efficient Visual Goal-Conditioned Reinforcement Learning using Object-Agnostic Masks

Fahim Shahriar^{1,4,*} Cheryl Wang^{2,*} Alireza Azimi^{1,4} Gautham Vasan^{1,4}
Hany Hamed Elanwar^{1,4} A. Rupam Mahmood^{1,4,5} Colin Bellinger^{3,4}

¹University of Alberta ²McGill University ³University of Ottawa ⁴AMII ⁵CIFAR Canada AI Chair ⁶Vector Institute
*Equal contribution.

{fshahri1, sazimi, vasan, hamed1}@ualberta.ca huiyi.wang@mail.mcgill.ca
armahmood@ualberta.ca colin.bellinger@uottawa.ca

Abstract—Goal-conditioned reinforcement learning (GCRL) allows agents to learn diverse objectives using a unified policy. The success of GCRL, however, is contingent on the choice of goal representation. In this work, we propose a mask-based goal representation system that provides object-agnostic visual cues to the agent, enabling efficient learning and superior generalization. In contrast, existing goal representation methods, such as target state images, 3D coordinates, and one-hot vectors, face issues of poor generalization to unseen objects, slow convergence, and the need for special cameras. Masks can be processed to generate dense rewards without requiring error-prone distance calculations. Learning with ground truth masks in simulation, we achieved 99.9% reaching accuracy on training and unseen test objects. Our proposed method can be utilized to perform pick-up tasks with high accuracy, without using any positional information of the target. Moreover, we demonstrate learning from scratch and sim-to-real transfer applications using two different physical robots, utilizing pretrained open vocabulary object detection models for mask generation.

I. INTRODUCTION

Many real-world robotics tasks, such as sorting objects in e-commerce warehouses or visual navigation to a target site, involve solving a multi-goal problem. These tasks require the agent to act in a particular way among numerous options to achieve various desired outcomes. Goal Conditioned Reinforcement Learning (GCRL) enables multi-goal learning by allowing the agent to acquire the necessary skills to solve a range of objectives, using a unified policy.

Goal representation plays a key role in GCRL. The choice of goal representation affects essential components of robot learning, such as convergence speed, learned behavior, and generalization capabilities [1], [2]. Goals can be represented in numerous ways, such as vectorized position or orientation, text, or target state image [2]. For object reaching and manipulation tasks, target position and orientation provide information-rich goal conditions that enable the agent to learn the task efficiently. In a real-world robotics setting, however, depth data processing techniques, such as feature matching and outlier rejection, are required to estimate the target position and orientation [3]. The accuracy of these values is significantly impacted by lighting, reflectivity, distance, and transparency of the target [3]. Other common goal representations, such as target image and text, are easier to

apply, but these representations inhibit the agent’s ability to generalize to new targets.

We propose a mask-based goal representation that is ideal for multi-goal and visual robotic reaching, manipulation, and navigation tasks. Our proposed method adds a binary channel to the agent’s visual input detailing the target. The mask is updated at each time step to provide the agent with object-agnostic visual cues and progression towards the target. In addition, this representation allows the agents to generalize to unseen targets, indicating robust generalization capability. Our experiments show that the mask-based goal representation matches or outperforms existing methods in visual reaching tasks with both training and unseen targets.

Sparse reward is a common challenge in GCRL, as it requires the agent to execute a long sequence of correct actions before receiving positive feedback [4]. This leads to poor sample efficiency and the failure to learn complex tasks. Dense reward, particularly distance-to-goal-based reward, is commonly used to mitigate this problem [5]. However, it often introduces new local optima that strongly depend on the environment and task definition, ultimately preventing agents from learning the optimal behavior [5].

In this work, we show that mask size can be used as an effective dense reward signal, since the target mask changes size and location based on the position of the target throughout the episode (Figure 4). Using mask-based reward removes the dependency on computing the target’s 3D world position, significantly simplifying real-world implementation. Mask-based goal conditioning and reward signals form a novel combination, and our experiments show that our proposed method outperforms existing approaches in a visual grab-and-pick-up task, learning from scratch. Although ideas similar to masks, such as segmentation masks, are present in the literature, our approach is novel because it uses a dynamic mask to track target progression and generate dense reward signals based on mask sizes.

We demonstrate that pretrained object detection models such as Detic [6] and Grounding DINO [7] can be used for mask generation in real-world tasks. We show the feasibility of using these pretrained models on two real-world applications: a) UR10e arm-based sim-to-real transfer, and

b) learning from scratch using the Franka Panda arm.

Our main contributions include: (1) the introduction of object masking as a goal representation strategy in vision-based GCRL; (2) an effective mask-based reward signal that minimizes the need for privileged information; (3) performing visual pick-up utilizing region-of-interest-based masks; (4) demonstrating the effectiveness of the proposed method in a sim-to-real and a real-world learning from scratch tasks.

II. RELATED WORK

Goal Representations: Vectorized position or orientation of an object or the robot is a common goal representation system used in the GCRL literature [8]–[10]. Other vectorized goal representations include one-hot encoding [11], [12], and object text description to CLIP embeddings [13]. For visual tasks, a common approach is to use variational autoencoders (VAE) to encode visual inputs such as RGB images into a latent space [14], [15]. However, traditional image-based goal conditioning tasks require a predefined goal state, which is unfeasible for tasks where such conditions are unknown and require exploration by the agent. In contrast, masks are simpler to generate and provide richer state-dependent feedback to the agent.

Mask-based Goal Representation. Object masking has been applied by researchers to represent target objects and goal positions under stationary camera configurations [16], [17]. These approaches train VAEs to encode images into latent vectors prior to GCRL training and use a latent state-based reward. On the other hand, our approach learns directly from images captured using an onboard camera. We use masks to track progression toward the target, and use mask-size-based rewards, which simplifies the learning process.

Yenamandra *et al.* used segmentation masks and depth data for target object finding and reaching tasks [13]. Stone *et al.* used masks with single activated pixels to denote target objects, allowing good generalization to objects of any shape and unseen objects [18]. Mendonca *et al.* used object masks to obtain the target object’s point-cloud information to perform mobile manipulation tasks [19]. Unlike these prior works, we include dynamic masks into the state space and leverage them to generate dense reward signals, an approach that enables robust goal representation and fast convergence.

Sparse Reward Challenge for GCRL: Sparse reward-based GCRL tasks often face an efficiency issue, as it takes a very long time for the reward signal to propagate from the goal states to the starting states [2], [20]. One approach to tackle this challenge is the use of distance-based dense rewards in either Euclidean space or latent space [8], [14], [15]. Nevertheless, this simple reward shaping is vulnerable to local optima that stem from a poor exploration of the environment [4]. Alternatively, hindsight experience replay (HER) addresses the sparse reward issue by re-assigning failed states as alternative goals and providing denser reward signals to speed up learning [20]. However, the HER-based approach still suffers from sample efficiency in complex environments [21]. For vision-based tasks, imagined sub-goals between the current and final goal state can sim-

plify learning for long-horizon tasks [14], [22], but these predictions sometimes result in unfeasible robotic states or unrealistic images.

Object Detection Models in Robotic Tasks: For vision-based robotic tasks, a common practice is to use object detection models to locate objects of interest. YOLO models are a common choice for researchers, due to their fast inference times and good accuracy [23], [24]. However, YOLO models support a fixed number of predefined object detections. As a result, users are required to retrain or fine-tune YOLO models to support novel objects [25], [26]. Recently, open vocabulary-based object detection models have gained popularity in the robotics community due to zero-shot detection capabilities. Open vocabulary object detectors, such as Detic and Grounding DINO, have been used in various robotic manipulation tasks [13], [18], [19]. In this work, we utilize pretrained open-vocabulary detection models to generate masks for goal conditioning and reward computation and to assess their feasibility in real-world tasks.

III. BACKGROUND

In standard RL, the objective is to train a policy to maximize the expected return. GCRL policies have a similar objective, but the expected return in each episode is conditioned on a predetermined goal $g \in \mathcal{G}$. GCRL can be formally represented by the goal-augmented Markov decision process (GA-MDP). At each time-step t , the agent samples an action $A_t \in \mathcal{A}$ based on the current state $S_t \in \mathcal{S}$, and the current goal g , using a policy π_ϕ , $A_t \sim \pi_\phi(\cdot | S_t, g)$. The agent receives a reward R_{t+1} and the next state S_{t+1} at the next time-step $t + 1$ based on a transition function P , $S_{t+1}, R_{t+1} \sim P(\cdot, \cdot | S_t, A_t, g)$. The episode ends when the agent reaches the goal, exceeds the allowed time limit, or leaves the allowed state space.

In this work, we evaluate the mask-based goal representation using on and off-policy methods. A brief overview of each method is provided below. Readers are directed to the original papers [27], [28], for more details.

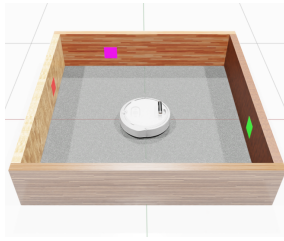
Soft Actor-Critic (SAC) is widely used for vision-based robotic tasks due to its higher sample efficiency. In GCRL, SAC learns the parameters ϕ of a policy π_ϕ to maximize a trade-off between the policy’s entropy and expected return. SAC uses a soft-Q function (critic) $Q_\theta(S_t, A_t, g)$, parameterized by θ , to estimate expected returns and the entropy bonus based on the current state, action, and goal.

Proximal Policy Optimization (PPO) is another frequently used RL algorithm for robotics tasks, particularly for sim-to-real applications. PPO updates policy parameters ϕ by maximizing the PPO-Clip objective and constraining changes to the new policy, improving the learning stability. PPO uses an advantage estimate \hat{A}_t that denotes how good the selected action a_t is in the current state S_t , and learns to increase the probabilities of selecting good actions. The critic function $V_t(S_t, g)$ predicts the expected return for a given state and goal, and it is used to generate accurate advantage estimates.

For vision-based GCRL tasks, the state S_t generally consists of an image I_t and a vector v_t , $S_t = \langle I_t, v_t \rangle$. An image



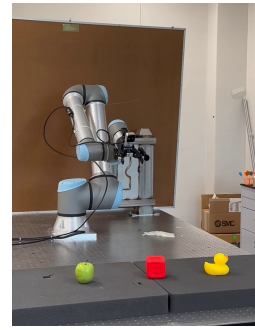
(a) Franka-MuJoCo environment. Example object names: chocolate donut, banana, and red apple.



(b) Create3-Isaac Sim environment.



(c) Learning from scratch setup with the Franka arm.



(d) Sim-to-real setup with the UR10e arm.

Fig. 1: Simulated and real-world environments.

encoder $f_\psi : \mathbb{R}^{H \times W \times C} \rightarrow \mathbb{R}^d$ is used to process the image into a lower dimensional latent vector; here ψ represents the learnable parameters, d is the latent dimension, and H , W , and C denote the height, width, and the number of channels of the input image respectively. Both the policy π_ϕ and the critic Q_θ use f_ψ to process the image, but the parameter ψ is only updated during the critic update.

Reward Systems: In GCRL, sparse rewards are only provided to the agent upon task completion:

$$R^{sparse}(s_t, a_t, g) = R^{\text{term}} \{ \text{goal reached} \}. \quad (1)$$

Distance-to-goal-based dense reward systems are often used as an alternative to the sparse reward system:

$$R^{dist}(s_t, a_t, g) = \begin{cases} -d(S_t, g) & \text{if } d(S_t, g) > \epsilon, \\ -d(S_t, g) + R^{\text{term}} & \text{if } d(S_t, g) \leq \epsilon. \end{cases} \quad (2)$$

Here, $d(S_t, g)$ denotes the distance to the goal for the state S_t , ϵ is the minimum distance to the goal, and R^{term} denotes a terminal reward.

IV. MASK-BASED VISUAL GCRL

Our proposed mask-based GCRL system comprises a novel mask-based goal representation and reward formulation, as well as specific enhancements to the learning algorithm for stable visual learning.

A. Mask-based Goal Representation

Masks are single-channel, binary images with the goal represented by a region of activated pixels. At each time step t , a mask m_t is created using the image from a camera sensor I_t^{cam} . The ground truth mask can be generated using privileged positional information of the target in simulation. Alternatively, object color-based or shape-based segmentation or pretrained object detectors can be used to generate masks. The mask is then appended to I_t^{cam} on the channel axis, to form $I'_t = [I_t^{cam} m_t]_C$. Three of the most recent such images are stacked on the channel axis to form I_t , where $I_t = [I'_t I'_{t-1} I'_{t-2}]_C$, and have the shape $90 \times 160 \times 12$, representing height, width, and channel.

Mask-based goal representation offers several advantages (demonstrated in Section VI): (1) the mask is calculated at each time step, providing richer signals and enabling faster training. (2) It is object-agnostic and facilitates better generalization to novel objects. (3) Masks can be generated

in multiple ways, and we demonstrate three such approaches: (a) using privileged object position, (b) using object detection models, and (c) using color filtering.

B. Mask-based Reward Formulation

The mask-based reward system serves as an alternative to the distance-based reward. Mask-based reward system replaces the distance to the goal term, $-d(S_t, g)$, in Equation (2) with R^{mask} :

$$R' = \frac{1}{H \times W} \sum_{i=1}^H \sum_{j=1}^W \mathbb{1}\{m_t^{ij} > 0\}, \quad (3)$$

$$R^{mask} = \frac{2}{1 + e^{-10 R'}} - 1. \quad (4)$$

Here, H and W are the height and width of the mask m_t , respectively. Equation (3) computes a normalized reward, R' , based on the activated pixels in m_t . Equation (4) applies a scaled sigmoid function to R' , which increases its value for small inputs, specifically when $R' < 0.5$. This scaling provides stronger feedback to the agent, particularly when the goal is further away and the changes in the mask sizes are small. R^{mask} is in the range $[0, 1]$.

C. Visual Learning Architectures

1) **SAC:** Our SAC implementation utilizes asynchronous network updates and replay buffer sampling to enable efficient learning in simulation and the real world [29]. To stabilize learning from pixels and to achieve better learning performance, we incorporated random shift [30], used an ensemble of five Q-Networks [31], and weight clipping [32] with $\kappa = 2$ and $s_t = \sqrt{2}$ in our SAC implementation. All experiments in our work, except sim-to-real on UR10e (VII-A), utilize SAC-based GCRL agents.

2) **PPO:** For the sim-to-real application, we used the Stable Baselines 3 implementation of PPO [33]. We chose PPO as it is widely used in sim-to-real tasks [34]. We used a novel image interpolation technique for training the PPO agent, which was essential to address visual domain shift during real-world policy transfer. We provide more details on this approach in Section VII-A.

V. EXPERIMENTAL SETUP

Here, we describe other goal representations, details of the environments used, and the details of the experiments to address a sequence of research questions.

Other Goal Representations: The **target state** goal representation adds a pre-existing close-up RGB image of the target with size $90 \times 160 \times 12$ to the stacked image states, I_t . **One-hot encoding**, **3D position**, and **CLIP embedding** are vector-based goal representations and appended to the vector part of the state space, v_t . One-hot encoding uses a 20D zero vector with a single activated index that identifies the target. CLIP embedding uses a 512D vector generated using a pretrained CLIP encoder based on a text description of the target object [13]. 3D position uses the privileged world position of the target collected from the simulator.

A. Environments

1) **Franka-MuJoCo Environment:** We created a tabletop setup with a Franka Panda robotic arm collected from MuJoCo Menagerie [35], and 20 everyday objects using Robohive [36], a MuJoCo-based robot learning framework. Figure 1a shows the simulated environment with all the objects placed on the tabletop. We attached a camera near the end-effector of the arm to facilitate vision-based reach, grasp, and lift. During training, three to five objects are arbitrarily selected from a pool of fifteen objects in each episode. The remaining five objects are held out as test objects. The selected objects are placed randomly on the table in front of the arm, and one object is randomly selected to be the target.

The goal of the GCRL agent for this task is to control individual joints of the Franka arm using low-level velocity commands to reach the target object within 150 time steps. The common state space across experiments contains a stack of the three most recent camera images of the shape $90 \times 160 \times 9$, the joint positions, and the last action.

2) **UR10e-MuJoCo Environment:** For this environment, we replaced the Franka arm with the UR10e arm (MuJoCo Menagerie). All other aspects of the environment remained the same. The joint lengths, angular velocities, and orientation of the joints for the UR10e arm are substantially different compared to the Franka arm. Furthermore, the UR10e arm is more sensitive to actions compared to the Franka arm, making the learning task slightly more difficult.

3) **Create 3-Isaac Sim Environment:** We created a square arena in the Isaac Sim simulator [37] and used an iRobot Create 3 mobile robot to test the visual navigation performance of the five goal conditioning methods. In each episode, we placed randomly chosen colored stickers (magenta, green, red, or blue) on each wall of the arena, and assigned a random pose to the Create 3 (Figure 1b). The GCRL agent needs to control the linear and angular velocities of the Create 3 to reach the selected target sticker in 200 time steps. We used three stacked images and a vectorized history, v_t , of the last 15 actions made by the agent. This allows the agent to have access to detailed information about the past motions of the robot. For this environment, we used color-filtering techniques to generate the masks.

In addition to these environments, in Section VII, we demonstrate sim-to-real transfer and learning from scratch on the UR10e and Franka Panda robots.

B. Research Questions

We aim to answer the following research questions:

1. Does the mask-based system enable (a) faster training, and (b) better generalization to unseen objects?
2. Is mask-based reward a viable alternative to distance-based dense reward?
3. Is it possible to use mask-based GCRL and reward systems for performing complex tasks, such as picking up?

C. Experiments

We design a sequence of experiments that address each of the research questions above.

Experiment 1 (a): To demonstrate the learning efficiency of the mask-based system, we trained mask-based GCRL agents in *Franka-MuJoCo*, *UR10e-MuJoCo*, and *Create3-Isaac Sim* environments and compared the learning performance against one-hot encoding, 3D position, CLIP embeddings, and target state-based goal representation systems. We used the distance-based dense reward defined in Equation (2), with ϵ set to 10 cm, and $R^{term} = 5$ for these experiments. Each experiment used eleven seeds, and we trained each agent for 300,000 steps. We used a replay buffer of size 300,000, and the initial 5,000 steps were used to pre-fill it.

Experiment 1 (b): We tested the reaching capabilities of the agents trained in *Experiment 1 (a)* for both seen and unseen objects for the *Franka-MuJoCo* and *UR10e-MuJoCo* environments. We ensured similarity across the experiments by selecting the five test objects deterministically based on the seed. To collect the reaching accuracy, for each seed, we carried out twenty-five trials for each object, resulting in a total of 5,500 trials for each goal representation system.

Experiment 2: In this experiment, we show that mask-based reward is a viable alternative to the distance-based reward. We trained mask-based GCRL agents with mask-based rewards on the *Franka-MuJoCo* and *UR10e-MuJoCo* environments and compared their performance against the mask-based GCRL agents with distance-based rewards from *Experiment 1 (a)*. The mask-based reward is calculated according to Equation (4), with an added -1 reward per step to facilitate faster training. We used the same settings defined in *Experiment 1 (a)* for the two environments.

Experiment 3: In this experiment, we demonstrate that mask-based GCRL agents can learn a complex visual pick-up task from scratch. The objective of the GCRL agent is to grab a target object placed randomly on a table and lift it up 30 cm above the table’s surface. We used a modified version of the *UR10e-MuJoCo* environment for this experiment. We used six objects out of 20 for the pick-up targets, which are: apple, green block, donut, toy duck, banana, and white egg. These objects were slightly scaled down in size to facilitate easier grasping. The other 14 objects were used as distractors during training, and in each episode, 2 to 4 objects were randomly sampled and placed on the table.

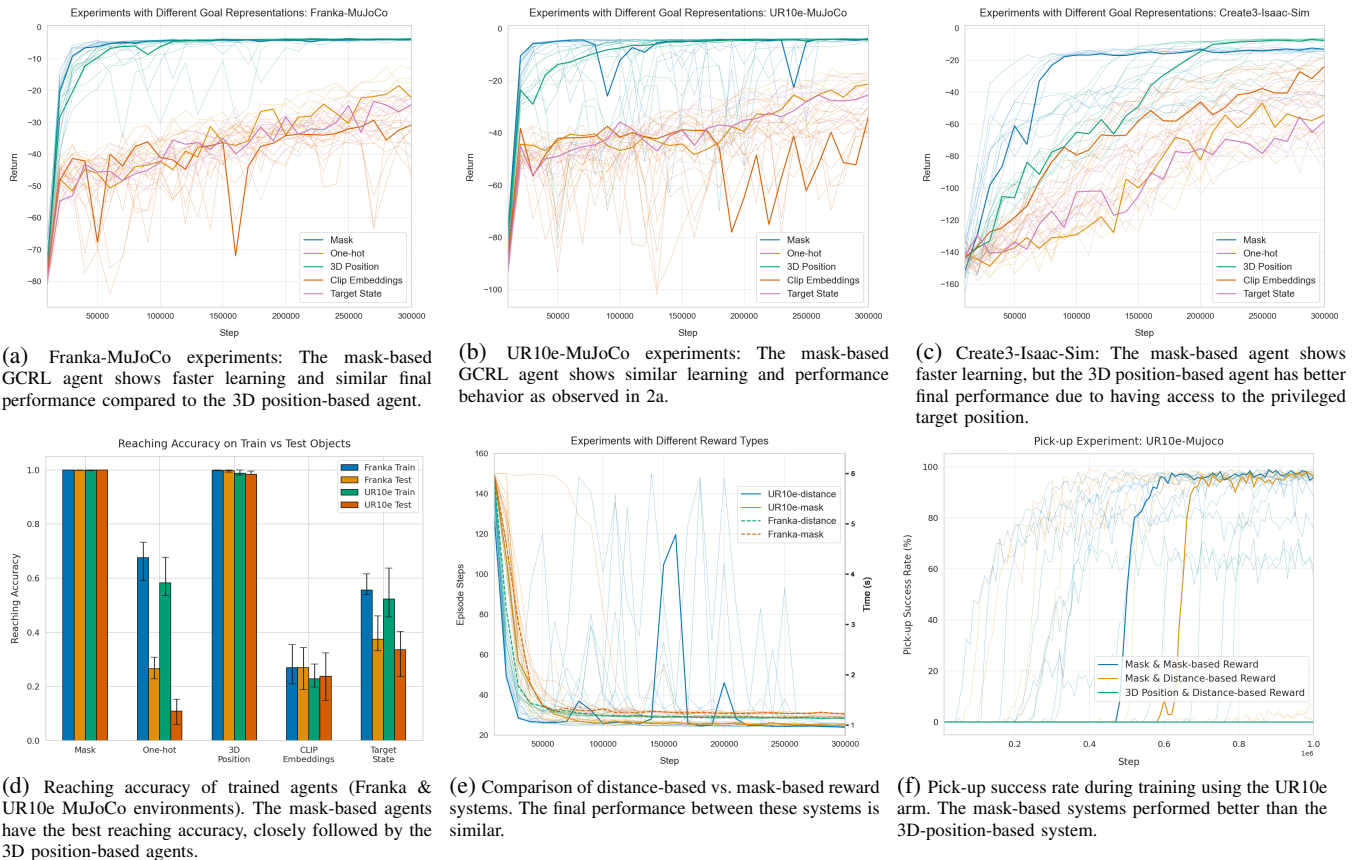


Fig. 2: Simulated experiment results

We compared the performance of mask-based goal conditioning (GC) and mask-based reward system with mask-based GC and distance-based reward system, and 3D position-based GC and distance-based reward system. For the mask-based GC, we selected the part of the image between the gripper fingers as the region of interest (ROI). This is where the object is expected to be during a successful grasp (Figure 4). The agent received the mask-size reward only if the target mask was inside the ROI. This approach allowed the agent to better align the robotic arm’s fingers with the target for good grasping, resulting in more successful pick-ups. For all three systems, we included the touch information of the target object and the arm’s fingers using a binary vector of size 2. For the mask-based system, once both fingers touched the target object, the mask activation was removed, and only a blank mask was provided. We trained the agents for one million steps, and the first 5000 steps were used to pre-fill the replay buffer, which had a size of 300,000.

We used the following reward function for this experiment:

$$R^{\text{pick}} = -1.1 + R^{\text{reach}} + R^{\text{contact}} + R^{\text{lift}} + R^{\text{goal}} \quad (5)$$

Here, R^{reach} is set to distance-based reward (Equation 2) or mask-based reward (Equation 4), and only applied before the agent touches the target with both fingers. R^{contact} is 10 for the first time both fingers touches the target and 0.1 for subsequent touches with both fingers. R^{lift} is set to $1 - 3.3 \cdot (D)$, where D is the current distance to the target height. R^{lift} is used after both fingers touch the target object. R^{goal}

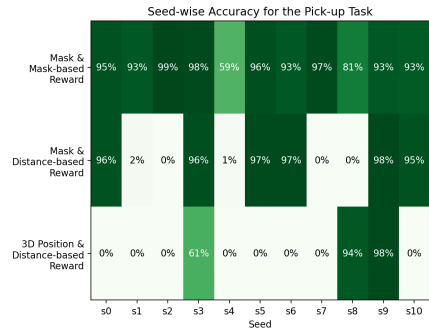
is a one-time reward of 10 upon reaching the target height.

After the training was completed, we used the trained policy to perform 50 pick-up trials for each object.

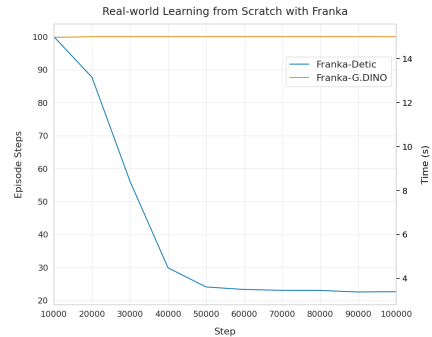
VI. RESULTS

Experiment 1 (a): Figure 2a, 2b, and 2c show the results for *Experiment 1 (a)*. The bold lines show the learning performance of the median run selected based on the episodic return, and the faint lines represent the remaining seeds. In all three experiments, the mask-based system achieved the fastest learning performance due to the rich feedback provided by the dynamic mask. For the *Franka-MuJoCo* and the *UR10e-MuJoCo* runs, the mask-based GCRL agent learned the optimal policy similar to the 3D position system. For the *Create3-Isaac Sim* experiments, the overall performance of the mask-based approach was slightly lower than the 3D-position method. This is because, for the 3D position, the agent always had access to the privileged target position, allowing it to learn to reach the target directly, even when not in view. On the other hand, for the mask-based method, the agent learns two skills: first, to find the target by rotating, and second, to move close to the target. Approaches such as one-hot encoding, CLIP embeddings, and target state showed poor learning performance, revealing the importance of selecting the appropriate goal conditioning method to achieve fast policy convergence.

Experiment 1 (b): Figure 2d shows the results for *Experiment 1 (b)*. The bars in the plot represent the median reaching accuracy, and the whiskers represent the first and



(a) Success rate of the trained agents in the post-training trials.



(b) Real-world experiments with Detic and Grounding DINO. For our real-world setup (1c), Detic-based agent performed much better than Grounding DINO.

Fig. 3: (a) Trial results for Experiment 3, (b) Learning curves for the real-world learning from scratch task.

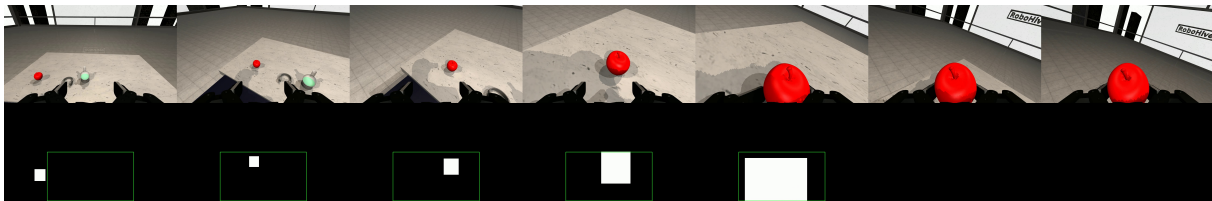


Fig. 4: A trained mask-based GC and reward agent successfully picks up the apple object. The green rectangles in the masks (bottom images) represent the ROI (shown only for illustration). In the last two frames, the agent lifts up the apple object after a successful grasp.

third quartiles. The mask-based GCRL agents achieved the highest performance for train and test objects, with 99.9% average accuracy for both. 3D position, on the other hand, achieved 98.9% and 98.8% average accuracy for train and test, respectively. This result shows that the agents learned to utilize the masks effectively for both train and test objects.

Experiment 2: In Figure 2e, we used average episode steps instead of return for comparison, as the distance-based and mask-based rewards are not directly comparable. The median runs are selected based on average episodic steps. The mask-based reward system performed similarly to the distance-based reward system while having higher stability during training. This result shows that the mask-based reward system is a viable alternative to the distance-based reward.

Experiment 3: Figure 2f shows the pick-up accuracy during training, and Figure 3a shows the pick-up accuracy of the trained agents. Nine out of eleven seeds for the mask-based GC and rewards system achieved over 90% pick-up success. On the other hand, only two seeds for the 3D position-based GC and distance-based reward system achieved over 90% success. This result shows that the ROI based masks guided the arm to a good grasp position (Figure 4), which resulted in higher pick-up accuracy. The 3D position-based systems did not have any grasping guidance, and the agent often failed to properly grasp the target, resulting in lower pick-up success. This experiment demonstrates that the mask-based system can be trained to perform complex visual pick-up tasks from scratch and shows the robustness of our proposed system.

VII. REAL-WORLD APPLICATIONS

Here, we provide two real-world applications of our system: sim-to-real transfer and real robot learning from scratch.

A. Sim-to-Real Application on UR10e

To assess the real-world applicability of our mask-based GCRL system, we performed a sim-to-real transfer of the proposed algorithm onto a physical UR10e robot (Figure 5b). The policy was trained using PPO in the *UR10e-MuJoCo* environment with the addition of domain randomization. We trained PPO with a custom multi-input policy using three-frame stacking and four parallel environments. We used ground-truth masks in simulation, where the privileged target information is readily available, and utilized Grounding DINO for mask generation in the real world. Grounding DINO uses (480×848) resolution images from a wrist-mount RealSense D435 camera. These are rescaled to 120×212 as input to the PPO CNN network. The best-performing policy from 10 seeds was selected for zero-shot transfer.

Domain randomization techniques are used to mitigate the discrepancies between simulated environments and the real world. The UR10e robot’s joint readings received Gaussian noise $\sim \mathcal{N}(0, 0.05)$ while its initial qpos varied by ± 0.2 for the first 5 DoFs. RGB images were augmented with contrast, saturation, brightness, and Gaussian blur (σ), all randomized within $[0.8, 1.2]$ using Kornia [38]. As shown in Figure 5a, we introduce a novel image augmentation process to reduce the image domain shift by linearly interpolating simulation images with randomly selected images from diverse real-world robotics tasks during training. This image augmentation was found to be essential for policy transfer.

We evaluate our system using in-distribution objects (green apple, red cube, yellow rubber duck) and two out-of-distribution test sets (Demo 1: toy robot, frog, water bottle; Demo 2: toy robot, plush dinosaur, water bottle). These objects were selected to provide variation in mass, size, color,

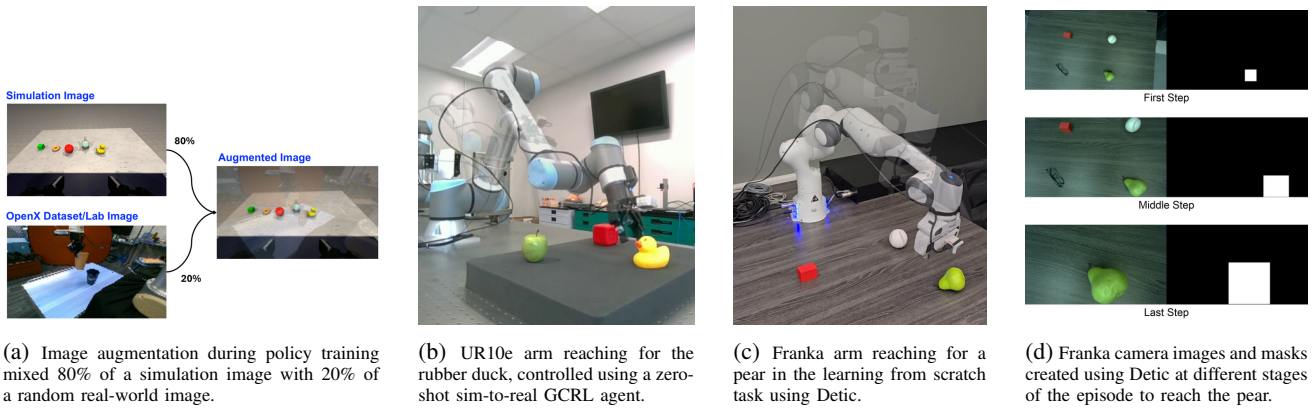


Fig. 5: Sim-to-real using UR10e and real-world learning from scratch using Franka.

shape, and surface texture, thereby thoroughly testing the generalization capabilities of our vision-based policy. The objects are randomly placed on the lab table.

TABLE I: Performance Comparison Between In-Distribution and Out-of-Distribution (OOD) Objects. Results obtained frame skip of 4 ms on UR10e with 25 trials each. We classify a trial as successful if the end effector reaches within 15 cm of the target object.

Metric	In-Distribution	OOD (Demo1)	OOD (Demo2)
Success Rate (%)	96	92	92
Distance (cm)	0.076 ± 0.035	0.13 ± 0.07	0.092 ± 0.050

Table I demonstrates successful real-world transfer of the policy, which achieves a success rate that is on par with its performance in simulation with ground-truth masks (89% for in distribution and 90% for out of distribution). The end-effector can reach within 15 cm of the target objects, regardless of their size and location.

We performed two additional tasks in the real world using the pretrained policy. We conducted pick-and-place by coupling a heuristic grab, lift, and place mechanism with the reaching policy. We also performed a tracking task by placing a target object in front of the arm and moving it gradually. The agent executed both tasks successfully, showing the robustness of the pretrained policy and Grounding DINO’s ability to generate masks for GCRL in the real world.

B. Learning from Scratch with Franka

We show the application of the mask-based system (goal representation and reward) in a real-world learning from scratch task using the Franka Panda arm (Figure 1c). We simplified the reaching task in the real world by using four stationary objects placed on a table in front of the arm: a red block, a baseball, a pear (artificial), and eyeglasses. We used Detic and Grounding DINO models for object detection and used slightly lower resolution images (450×800) to facilitate faster inference times. We used 100 steps per episode and trained for 100,000 steps. The termination distance, ϵ , was set to 13 cm from the target. We used an Intel RealSense D405 camera attached near the end-effector of the arm to capture images. We performed the training on a computer equipped with a Ryzen Threadripper 3970X processor and an Nvidia

RTX 3090 GPU. We used the same SAC GCRL system that we used in the simulated experiments. The GCRL agent had to learn to reach the randomly selected target object by controlling the joint velocities of the arm.

Figure 3b shows the results of the real-world learning from scratch experiments. The Franka-Detic agent learned an optimal reaching policy in 60,000 steps. Figure 5c shows the trained agent reaching for a pear, and Figure 5d shows the associated camera images and masks generated using Detic. On the other hand, the Grounding DINO model had severe false-positive detection issues. The agent failed to reach the target objects as it tried to exploit rewards from false detection masks. This experiment show the possibilities and difficulties of using pretrained object detection models in real-world learning from scratch tasks.

We further evaluated the trained Detic-based GCRL agent by performing a tracking task with an unseen object. We placed a plastic banana on top of the table and moved it using a stick while the GCRL agent was controlling the arm. The agent managed to follow the banana easily, even though it was trained on reaching stationary objects. The successful tracking behavior demonstrates the robustness and the generalization capabilities of our proposed system.

VIII. CONCLUSION

In this work, we introduced an object-agnostic mask-based GCRL and reward system. We showed that our proposed system performs better than other approaches in visual manipulation tasks and performs similarly in reaching tasks. The mask-based systems showed superior reaching performance on novel objects utilizing RGB images only, achieving 99.9% accuracy. Moreover, we showed that dense reward based on mask size is an effective alternative to distance-to-target-based reward, diminishing the necessity for distance calculation methods. The mask-based agents performed exceptionally well in the visual pick-up task. Finally, we showed that our proposed method is effective in real robot learning, and open-vocabulary object detection models are effective when transferring trained policies from simulation to real robots.

REFERENCES

- [1] T. Schaul, D. Horgan, K. Gregor, and D. Silver, “Universal value function approximators,” in *Proceedings of the 32nd International Conference on Machine Learning*, ser. Proceedings of Machine Learning Research, F. Bach and D. Blei, Eds., vol. 37. Lille, France: PMLR, 07–09 Jul 2015, pp. 1312–1320. [Online]. Available: <https://proceedings.mlr.press/v37/schaul15.html>
- [2] M. Liu, M. Zhu, and W. Zhang, “Goal-conditioned reinforcement learning: Problems and solutions,” in *Proceedings of the Thirty-First International Joint Conference on Artificial Intelligence, IJCAI-22*, L. D. Raedt, Ed. International Joint Conferences on Artificial Intelligence Organization, 7 2022, pp. 5502–5511, survey Track. [Online]. Available: <https://doi.org/10.24963/ijcai.2022/770>
- [3] X. Dong, M. A. Garratt, S. G. Anavatti, and H. A. Abbass, “Towards real-time monocular depth estimation for robotics: A survey,” *IEEE Transactions on Intelligent Transportation Systems*, vol. 23, no. 10, pp. 16 940–16 961, 2022.
- [4] G. Vasan, Y. Wang, F. Shahriar, J. Bergstra, M. Jägersand, and A. R. Mahmood, “Revisiting sparse rewards for goal-reaching reinforcement learning,” *Reinforcement Learning Journal*, vol. 4, pp. 1841–1854, 2024.
- [5] A. Trott, S. Zheng, C. Xiong, and R. Socher, “Keeping your distance: Solving sparse reward tasks using self-balancing shaped rewards,” *Advances in Neural Information Processing Systems*, vol. 32, 2019.
- [6] X. Zhou, R. Girdhar, A. Joulin, P. Krähenbühl, and I. Misra, “Detecting twenty-thousand classes using image-level supervision,” in *European conference on computer vision*. Springer, 2022, pp. 350–368.
- [7] S. Liu, Z. Zeng, T. Ren, F. Li, H. Zhang, J. Yang, Q. Jiang, C. Li, J. Yang, H. Su *et al.*, “Grounding dino: Marrying dino with grounded pre-training for open-set object detection,” in *European conference on computer vision*. Springer, 2024, pp. 38–55.
- [8] M. Plappert, M. Andrychowicz, A. Ray, B. McGrew, B. Baker, G. Powell, J. Schneider, J. Tobin, M. Chociej, P. Welinder *et al.*, “Multi-goal reinforcement learning: Challenging robotics environments and request for research,” *arXiv preprint arXiv:1802.09464*, 2018.
- [9] C. Florensa, D. Held, X. Geng, and P. Abbeel, “Automatic goal generation for reinforcement learning agents,” in *International conference on machine learning*. PMLR, 2018, pp. 1515–1528.
- [10] Y. Tang and A. Kucukelbir, “Hindsight expectation maximization for goal-conditioned reinforcement learning,” in *International Conference on Artificial Intelligence and Statistics*. PMLR, 2021, pp. 2863–2871.
- [11] D. Kalashnikov, J. Varley, Y. Chebotar, B. Swanson, R. Jonschkowski, C. Finn, S. Levine, and K. Hausman, “Scaling up multi-task robotic reinforcement learning,” in *Proceedings of the 5th Conference on Robot Learning*, ser. Proceedings of Machine Learning Research, A. Faust, D. Hsu, and G. Neumann, Eds., vol. 164. PMLR, 08–11 Nov 2022, pp. 557–575. [Online]. Available: <https://proceedings.mlr.press/v164/kalashnikov22a.html>
- [12] Q. Wu, K. Xu, J. Wang, M. Xu, X. Gong, and D. Manocha, “Reinforcement learning-based visual navigation with information-theoretic regularization,” *IEEE Robotics and Automation Letters*, vol. 6, no. 2, pp. 731–738, 2021.
- [13] S. Yenamandra, A. Ramachandran, K. Yadav, A. Wang, M. Khanna, T. Gervet, T.-Y. Yang, V. Jain, A. W. Clegg, J. Turner, Z. Kira, M. Savva, A. Chang, D. S. Chaplot, D. Batra, R. Mottaghi, Y. Bisk, and C. Paxton, “Homerobot: Open vocabulary mobile manipulation,” 2023. [Online]. Available: <https://github.com/facebookresearch/home-robot>
- [14] A. V. Nair, V. Pong, M. Dalal, S. Bahl, S. Lin, and S. Levine, “Visual reinforcement learning with imagined goals,” *Advances in neural information processing systems*, vol. 31, 2018.
- [15] L. Cong, H. Liang, P. Ruppel, Y. Shi, M. Görner, N. Hendrich, and J. Zhang, “Reinforcement learning with vision-proprioception model for robot planar pushing,” *Frontiers in Neurorobotics*, vol. 16, Mar. 2022. [Online]. Available: <http://dx.doi.org/10.3389/fnbot.2022.829437>
- [16] Y. Wang, N. Gautham, X. Lin, B. Okorn, and D. Held, “Roll: Visual self-supervised reinforcement learning with object reasoning,” in *Conference on robot learning*. PMLR, 2021, pp. 1030–1048.
- [17] L. Cong, H. Liang, P. Ruppel, Y. Shi, M. Görner, N. Hendrich, and J. Zhang, “Reinforcement learning with vision-proprioception model for robot planar pushing,” *Frontiers in Neurorobotics*, vol. 16, p. 829437, 2022.
- [18] A. Stone, T. Xiao, Y. Lu, K. Gopalakrishnan, K.-H. Lee, Q. Vuong, P. Wohlhart, S. Kirmani, B. Zitkovich, F. Xia, C. Finn, and K. Hausman, “Open-world object manipulation using pre-trained vision-language models,” 2023. [Online]. Available: <https://arxiv.org/abs/2303.00905>
- [19] R. Mendonca and D. Pathak, “Continuously improving mobile manipulation with autonomous real-world RL,” in *RSS 2024 Workshop: Data Generation for Robotics*, 2024. [Online]. Available: <https://openreview.net/forum?id=qASoq07bXh>
- [20] M. Andrychowicz, F. Wolski, A. Ray, J. Schneider, R. Fong, P. Welinder, B. McGrew, J. Tobin, O. Pieter Abbeel, and W. Zaremba, “Hindsight experience replay,” *Advances in neural information processing systems*, vol. 30, 2017.
- [21] Y. Luo, Y. Wang, K. Dong, Q. Zhang, E. Cheng, Z. Sun, and B. Song, “Relay hindsight experience replay: Self-guided continual reinforcement learning for sequential object manipulation tasks with sparse rewards,” *Neurocomputing*, vol. 557, p. 126620, 2023.
- [22] E. Chane-Sane, C. Schmid, and I. Laptev, “Goal-conditioned reinforcement learning with imagined subgoals,” in *International conference on machine learning*. PMLR, 2021, pp. 1430–1440.
- [23] S. Uppal, A. Agarwal, H. Xiong, K. Shaw, and D. Pathak, “Spin: Simultaneous perception interaction and navigation,” in *Proceedings of the IEEE/CVF Conference on Computer Vision and Pattern Recognition*, 2024, pp. 18 133–18 142.
- [24] Y. Zhang, L. Ke, A. Deshpande, A. Gupta, and S. S. Srinivasa, “Cherry-picking with reinforcement learning,” in *Robotics: Science and Systems*, 2023.
- [25] Y.-L. Chen, Y.-R. Cai, and M.-Y. Cheng, “Vision-based robotic object grasping—a deep reinforcement learning approach,” *Machines*, vol. 11, no. 2, p. 275, 2023.
- [26] Q. Song, S. Li, Q. Bai, J. Yang, X. Zhang, Z. Li, and Z. Duan, “Object detection method for grasping robot based on improved yolov5,” *Micromachines*, vol. 12, no. 11, 2021. [Online]. Available: <https://www.mdpi.com/2072-666X/12/11/1273>
- [27] T. Haarnoja, A. Zhou, P. Abbeel, and S. Levine, “Soft actor-critic: Off-policy maximum entropy deep reinforcement learning with a stochastic actor,” in *International conference on machine learning*. Pmlr, 2018, pp. 1861–1870.
- [28] J. Schulman, F. Wolski, P. Dhariwal, A. Radford, and O. Klimov, “Proximal policy optimization algorithms,” *CoRR*, vol. abs/1707.06347, 2017.
- [29] Y. Yuan and A. R. Mahmood, “Asynchronous reinforcement learning for real-time control of physical robots,” in *2022 International Conference on Robotics and Automation (ICRA)*. IEEE, 2022, pp. 5546–5552.
- [30] D. Yarats, R. Fergus, A. Lazaric, and L. Pinto, “Mastering visual continuous control: Improved data-augmented reinforcement learning,” in *Deep RL Workshop NeurIPS 2021*, 2021. [Online]. Available: <https://openreview.net/forum?id=L5HKN-IsdSE>
- [31] X. Chen, C. Wang, Z. Zhou, and K. W. Ross, “Randomized ensembled double q-learning: Learning fast without a model,” in *International Conference on Learning Representations*, 2021. [Online]. Available: <https://openreview.net/forum?id=AY8zFzm0Dd>
- [32] M. Elsayed, Q. Lan, C. Lyle, and A. R. Mahmood, “Weight clipping for deep continual and reinforcement learning,” *RLJ*, vol. 5, pp. 2198–2217, 2024.
- [33] A. Raffin, A. Hill, A. Gleave, A. Kanervisto, M. Ernestus, and N. Dormann, “Stable-baselines3: Reliable reinforcement learning implementations,” *Journal of Machine Learning Research*, vol. 22, no. 268, pp. 1–8, 2021. [Online]. Available: <http://jmlr.org/papers/v22/20-1364.html>
- [34] W. Zhao, J. P. Queralta, and T. Westerlund, “Sim-to-real transfer in deep reinforcement learning for robotics: a survey,” in *2020 IEEE symposium series on computational intelligence (SSCI)*. IEEE, 2020, pp. 737–744.
- [35] K. Zakka, Y. Tassa, and MuJoCo Menagerie Contributors, “MuJoCo Menagerie: A collection of high-quality simulation models for MuJoCo,” 2022. [Online]. Available: <http://github.com/google-deepmind/mujoco.menagerie>
- [36] “Robohive – a unified framework for robot learning,” 2020. [Online]. Available: <https://sites.google.com/view/robohive>
- [37] NVIDIA, “Isaac sim,” <https://developer.nvidia.com/isaac-sim>, 2025, version 4.5.0.
- [38] E. Riba, D. Mishkin, D. Ponsa, E. Rublee, and G. Bradski, “Kornia: an open source differentiable computer vision library for pytorch,” in *Winter Conference on Applications of Computer Vision*, 2020. [Online]. Available: <https://arxiv.org/pdf/1910.02190.pdf>